One-proton knockout from ^{17}N at 245 MeV/nucleon

T. Q. Liu,[1,2] S. T. Wang,[1,2,*] Z. Y. Sun,[1,2,†] Y. Z. Sun,[1] C. X. Yuan,[3] J. G. Li,[1,2] W. L. Hai,[4] D. Y. Pang,[4] X. H. Zhang,[1,2] D. Yan,[1,2] S. Y. Jin,[1,2] Y. H. Yu,[1,2] S. W. Tang,[1,2] H. J. Ong,[1,2] F. Fang,[1,2] Y. J. Zhang,[1,2] Y. F. Xu,[1,2] Z. Y. Li,[1,2] X. B. Wei,[1,5] F. H. Lu,[1,2] S. W. Fu,[1,2] and X. M. Liu[1,2,6]

[1]*Institute of Modern Physics, Chinese Academy of Sciences, Lanzhou 730000, China*
[2]*School of Nuclear Science and Technology, University of Chinese Academy of Sciences, Beijing 100049, China*
[3]*Sino-French Institute of Nuclear Engineering and Technology, Sun Yat-Sen University, Zhuhai 519082, China*
[4]*School of Physics and Beijing Key Laboratory of Advanced Nuclear Materials and Physics, Beihang University, Beijing 100191, China*
[5]*College of Physics, Henan Normal University, Xinxiang 453007, China*
[6]*School of Nuclear Science and Technology, Lanzhou University, Lanzhou 730000, China*

(Received 22 December 2023; accepted 14 May 2024; published 3 June 2024)

The cross section for one-proton knockout from ^{17}N on a carbon target at 245 MeV/nucleon has been measured. The experimental result is compared to the predictions based on the Glauber reaction model combined with shell model structure inputs. The experimental to theoretical cross section ratio R_s is consistent with the well established R_s-ΔS systematics. The experimental one-proton knockout cross section for ^{17}N projectile is found to be smaller than those for the neighboring isotones ^{16}C and ^{18}O. The observed small cross section for ^{17}N can be attributed to the small spectroscopic factors from ^{17}N to the bound states of ^{16}C residue. The shell model calculations show that one-proton removal from the $\pi 0p_{3/2}$ orbital of ^{17}N mainly leads to unbound states of ^{16}C, and the spectroscopic factor from ^{17}N to the ^{16}C 2_1^+ state is negligibly small, indicating that the proton configuration $\pi(0p_{3/2})^3(0p_{1/2})^1$ contributes little to the ^{16}C 2_1^+ state and neutron excitation configuration plays dominant role.

DOI: 10.1103/PhysRevC.109.064604

I. INTRODUCTION

The evolution of nuclear structure away from the stability line has drawn significant attention in nuclear physics [1–6]. When the proton or neutron number is the "magic number," large gaps exist between nuclear shells, resulting in large transition energy values between the ground and the first 2_1^+ excited states for doubly magic nuclei [1,7]. Therefore, for even-even nuclei, the nature of the first excited 2_1^+ states provides important information on the evolution of nuclear properties.

The carbon isotopes have a long isotopic chain, providing a good opportunity for the study of nuclear structure evolution toward the drip line [4]. The splitting of the $0p_{1/2}$-$0p_{3/2}$ orbitals in ^{12}C results in a large shell gap between them, manifested by the high-energy 2_1^+ state. It is revealed that the proton $0p_{1/2}$-$0p_{3/2}$ gap persists toward the neutron-rich ^{20}C [8]. While ^{12}C and ^{14}C have high-energy 2_1^+ states, ^{16}C has a relatively low 2_1^+ energy, implying that the neutron excitation plays the dominant role in the 2_1^+ state of ^{16}C.

One-nucleon knockout reactions induced by light composite nuclear targets, e.g., Be or C, have been extensively used to probe the structure of rare isotopes away from the stability line [9–13]. The structure of ^{16}C was recently studied using one-proton knockout from ^{17}N on a carbon target at 72 MeV/nucleon [14]. The relative cross section for populating the ^{16}C 2_1^+ state over the 0_1^+ state was measured in that work, while the absolute cross sections of these two states are missing. This paper reports a measurement of the inclusive cross section for one-proton knockout from ^{17}N on a carbon target with a higher beam energy of 245 MeV/nucleon. The knockout reaction model uses sudden and eikonal approximation (SE approximation) [15]. When knocking out a strongly bound proton in the neutron-rich ^{17}N nucleus, the high beam energy is important for the reliable applicability of the SE approximation. As is shown in Ref. [16], strong nonsudden effects are observed when knocking out a strongly bound neutron from ^{14}O at a beam energy of 57 MeV/nucleon. Thus, higher beam energy is favorable for one-proton knockout from ^{17}N to enhance the validity of the SE approximation. The present reaction is of sufficiently high beam energy to avoid any significant nonsudden dynamical effects.

II. EXPERIMENTAL DETAILS

The experiment was performed at the External Target Facility (ETF) [17] at the Institute of Modern Physics, Chinese Academy of Sciences. A secondary beam of ^{17}N was produced by fragmentation of a 280 MeV/nucleon ^{18}O primary beam, which was accelerated by the main Cooler Storage Ring (CSRm) synchrotron of the Heavy Ion Research Facility in Lanzhou (HIRFL) [18] and directed onto a 15-mm-thick Be

*wangshitao@impcas.ac.cn
†sunzhy@impcas.ac.cn

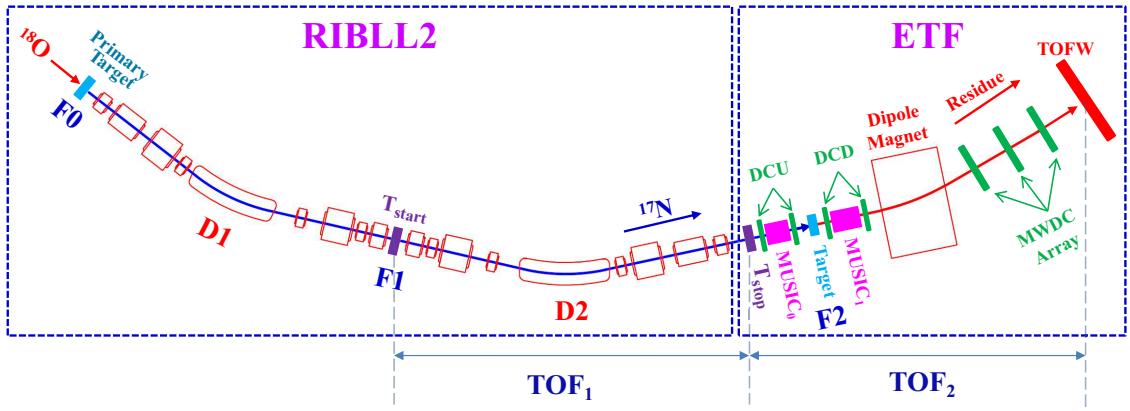

FIG. 1. Schematic view of RIBLL2 and ETF.

target. The desired ^{17}N fragment was separated and transported by the second Radioactive Ion Beam Line in Lanzhou (RIBLL2) [19] to the ETF to impinge on a 900-mg/cm^2 carbon target. The ^{17}N beam energy at the middle of target is 245 MeV/nucleon. The setups of RIBLL2 and ETF are illustrated in Fig. 1.

The secondary cocktail beams were identified by TOF-ΔE method. The time of flight (TOF$_1$) of secondary cocktail beams was measured by the two plastic scintillator detectors ($T_{\rm start}$ and $T_{\rm stop}$ [20]). The energy loss (ΔE_0) was recorded by the multiple sampling ionization chamber (MUSIC$_0$) [21] before the target. The particle identification (PID) spectrum of the secondary cocktail beams is presented in Fig. 2. Different nuclei can be separated clearly. Two multiwire drift chambers (DCU), each with an active area of 13 × 13 cm^2, were located upstream of the target to measure the trajectories of the incident particles.

Downstream from the reaction target, the reaction fragments and unreacted projectiles were identified event by event by the detector system of the ETF, using thee $B\rho$-TOF-ΔE method. Two multiwire drift chambers (DCDs) with the same 13 × 13 cm^2 active area and a multiple sampling ionization chamber (MUSIC$_1$) [22] behind the reaction target provided measurements of the trajectories and energy loss (ΔE_1) of the outgoing residues respectively. The outgoing residues were then deflected by a large acceptance dipole magnet and detected by the MWDC array [23] and the plastic scintillator wall (TOFW) [24] with 30 vertical strips, each having an active area of 4 × 120 cm^2. The trajectories of the charged residues after the magnet were reconstructed by the MWDC array [23], which has three MWDCs, and each of them has an active area of 80 × 60 cm^2. With the combination of the trajectories reconstructed by the DCD and MWDC array, the magnetic rigidity ($B\rho$) of the outgoing charged residues passing through the magnet can be determined. The TOF of residues (TOF$_2$) were measured by $T_{\rm stop}$ and TOFW. The atomic number Z of the residues can be obtained by using the ΔE_1 information, while the mass numbers A of the residues were determined by using the relation $B\rho \approx \beta\gamma A/Z$, where β and γ denote the velocity v/c and the Lorentz factor, respectively. A PID spectrum for carbon residues after ^{17}N impinging on the reaction target is displayed in Fig. 3, with an A resolution $\sigma_A/A \approx 0.01$. It can be seen that one-proton knockout products ^{16}C can be well separated from other carbon isotopes.

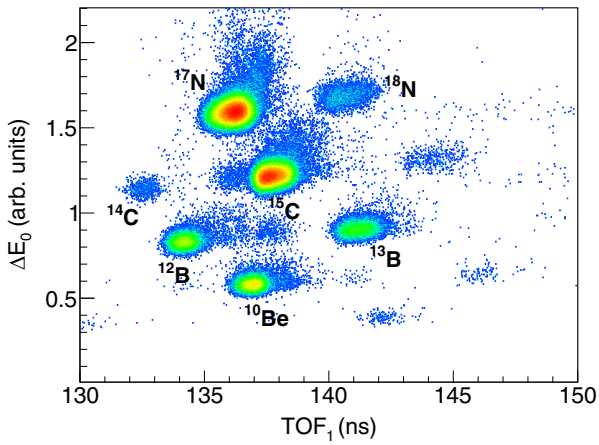

FIG. 2. Particle identification spectrum of the secondary cocktail beams.

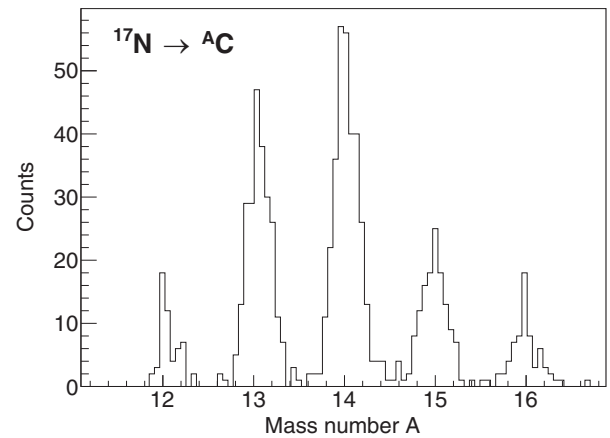

FIG. 3. Particle identification spectrum for carbon residues produced by ^{17}N reaction.

Because the ETF detector system has a large acceptance and the system is set for the transport of ^{16}C residues, the acceptance of the ETF detector system for the ^{16}C residues is ≈100%. The detection efficiency of the ETF was calibrated using the cocktail secondary beams without the reaction target. The obtained ^{16}C detection efficiency in the ETF is 90.5%.

The experimental one-proton knockout cross section of ^{17}N is achieved according to

$$\sigma_{\rm exp} = \frac{N_r}{N_p t \epsilon}, \tag{1}$$

where N_r and N_p are the numbers of ^{16}C residues and ^{17}N projectiles, respectively. t is the target nucleus density per area, and ϵ is the product of detection efficiency and geometric acceptance for ^{16}C. N_r and N_p can be obtained from the PID spectrum, and ϵ is 90.5%. The background contributions were measured by using target-out runs and subtracted.

The parallel momenta of the ^{16}C residues and the ^{17}N unreacted beams are deduced from

$$P_{//} = M\beta\gamma\cos(\theta), \tag{2}$$

where M is the mass of the nucleus, and θ denotes the angle between the direction of the incident ^{17}N projectile and the direction of the outgoing nucleus.

III. THEORETICAL CALCULATIONS

Based on the Glauber model combined with shell model input, the theoretical cross section of the one-proton knockout reaction is calculated by [25]

$$\sigma_{\rm th} = \sum_{nlj}\left[\frac{A}{A-1}\right]^N C^2S(J^\pi, nlj)\sigma_{\rm sp}\left(nlj, S_p^{\rm eff}\right), \tag{3}$$

where C^2S is the shell model spectroscopic factor for the removed proton with respect to the core state J^π, $\sigma_{\rm sp}$ denotes the single-particle cross section derived from the Glauber model using SE approximation, nlj are the quantum numbers of the removed proton, and $S_p^{\rm eff} = S_p + E^*$ is the effective proton separation energy to the bound final state J^π of the residue, with S_p the ground-state to ground-state separation energy of the valence proton and E^* the excitation energy of the residue in the J^π state. The $[A/(A-1)]^N$ is the center-of-mass correction factor with A the mass number of the projectile and $N = 2n + l = 0, 1, 2, \ldots$ the major oscillator quantum number of the removed proton. It can be seen that the theoretical cross section mostly depends on the spectroscopic factor C^2S and the single-particle cross section $\sigma_{\rm sp}$.

The spectroscopic factors from ^{17}N ground state to ^{16}C bound final states are computed with the code KSHELL [26], using the WBP and YSOX effective interactions [27,28]. The interactions are constructed in (0–5)$\hbar\omega$ *psd* model space, which means that 0–5 nucleons are allowed to be excited from *p* shell to *sd* shell.

The single-particle cross section $\sigma_{\rm sp}$, which is a sum of the contributions from two mechanisms [15], i.e., the stripping mechanism and diffractive dissociation mechanism, is calculated with computer code CNOK [29], a C++ program package implementing Glauber reaction model. The valence-proton wave function Ψ_{nlj} is calculated by employing a nuclear central potential of Woods-Saxon (WS) form plus a spin-obit interaction and a Coulomb potential. The shape of the WS potential, which is determined by its radius r_0, diffuseness a_0, and the depth V_0, is adjusted by a two-dimensional search in the (r_0, V_0) space of the central WS potential to reproduce the effective separation energy $S_p^{\rm eff}$ and $r_{\rm sp}$, two input quantities in the code. The same r_0 is used in the spin-obit interaction with potential depth $V_{\rm s0} = 7.5$ MeV and Coulomb potential. A diffuseness of $a_0 = 0.7$ fm is adopted for both the central potential and the spin-orbit interaction to get the Ψ_{nlj}. To obtain the rms radius of the valence proton wave functions, $r_{\rm sp} = [A/(A-1)]^{1/2} r_{\rm HF}$ [30], a Hartree-Fock (HF) calculation based on the SkX parametrization [31] is used to get $r_{\rm HF}$, the rms radius of the valence-proton orbital. The calculation is also taken for the determination of the nucleon density distribution of the residue and target nuclei, and the proton- and residue-target elastic S matrices are obtained using the nucleon density distribution of the residue and target nuclei via the t-ρ-ρ method [32].

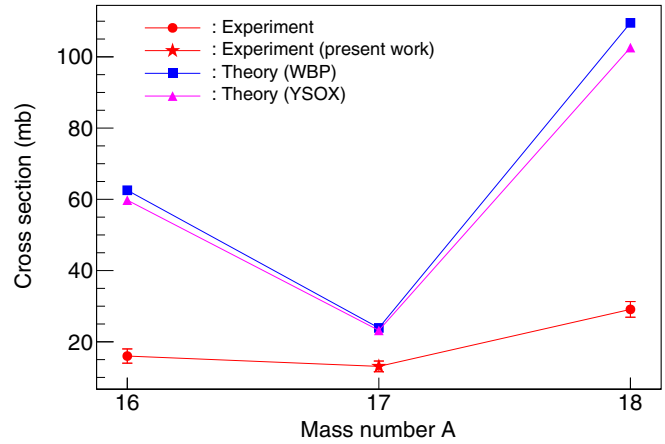

FIG. 4. Experimental and theoretical one-proton knockout reaction cross sections of ^{16}C, ^{17}N, and ^{18}O. Experimental cross sections of ^{16}C and ^{18}O are from Refs. [33] and [34], respectively.

The theoretical parallel momentum distributions of the ^{16}C residues in different bound final states, with the removal of an $l = 1$ proton from ^{17}N projectiles, are also calculated with CNOK. In the calculation, we used the same S matrices and C^2S inputs as employed in calculating theoretical cross section. The calculated momentum distributions are converted to the laboratory frame for a direct comparison with the measured distribution.

IV. RESULTS AND DISCUSSION

The experimental and theoretical cross sections for ^{17}N one-proton knockout at 245 MeV/nucleon are shown in Table I and Fig. 4. The inclusive experimental cross section is $\sigma_{\rm exp}(^{17}{\rm N} \rightarrow {}^{16}{\rm C}) = 13.1(15)$ mb.

For a systematic comparison, the existing data on one-proton knockout cross sections for the neighboring ^{16}C and ^{18}O isotones at similar beam energies, as well as the calculated

TABLE I. Inclusive experimental and theoretical one-proton knockout cross sections (σ_{exp} and σ_{th}) and the resulting reduction factors $R_s = \sigma_{exp}/\sigma_{th}$ for ^{16}C, ^{17}N, and ^{18}O. The values labeled WBP and YSOX correspond to the calculation results using the WBP and YSOX effective interaction respectively.

			E^*	S_p^{eff}	σ_{sp}	C^2S		$\sigma_{th(WBP)}$	$\sigma_{th(YSOX)}$	σ_{exp}	R_s	
Projectile	nlj	J^π	(MeV)	(MeV)	(mb)	WBP	YSOX	(mb)	(mb)	(mb)	WBP	YSOX
^{16}C	$0p_{3/2}$	$3/2^-$	0	22.55	20.59	2.85	2.72	62.54	59.77			
	inclusive					2.85	2.72	62.54	59.77	16.0(20)[a]	0.26(3)	0.27(3)
^{17}N	$0p_{1/2}$	0_1^+	0	13.11	21.72	0.77	0.76	17.70	17.44			
		0_2^+	3.03	16.14	21.63	0.004	0.007	0.09	0.16			
	$0p_{3/2}$	2_1^+	1.77	14.89	20.11	0.10	0.08	2.04	1.75			
		2_2^+	3.99	17.10	20.06	0.19	0.18	4.07	3.86			
	inclusive					1.06	1.03	23.90	23.21	13.1(15)	0.55(6)	0.56(6)
^{18}O	$0p_{1/2}$	$1/2_1^-$	0	15.94	24.17	1.69	1.65	43.37	42.17			
		$1/2_2^-$	3.66	19.61	20.49	0.03	0.04	0.74	0.77			
	$0p_{3/2}$	$3/2_1^-$	1.37	17.32	19.35	0.29	0.20	6.01	4.11			
		$3/2_2^-$	3.20	19.15	19.29	0.37	0.21	7.55	4.21			
		$3/2_3^-$	5.52	21.46	19.25	2.55	2.52	51.88	51.34			
	inclusive					4.93	4.62	109.55	102.60	29.1(22)[b]	0.27(2)	0.28(2)

[a]From Ref. [33].
[b]From Ref. [34].

values, are added in Table I and Fig. 4. The theoretical results with the WBP and YSOX effective interactions shown in Table I are quite similar. Therefore, only the calculations with the YSOX interaction are chosen for comparison with experimental results in the following discussion. It can be seen that the experimental one-proton knockout cross section for ^{17}N is lower than those for ^{16}C and ^{18}O. This feature is reproduced by the calculations, while quantitatively the experimental values are much smaller than calculated values. For the presently measured reaction (^{17}N, ^{16}C), the deduced reduction factor R_s, ratio of the experimental and theoretical inclusive cross sections, is 0.56(6).

A systematic analysis of a large body of one-nucleon knockout data [35] indicated that the reduction factor R_s has a strong dependence on the asymmetry of the neutron and proton separation energies ΔS. For one-proton knockout reaction, $\Delta S = S_p - S_n + \overline{E}^*$, where $\overline{E}^*$ is the averaged residue excitation energy weighted by the calculated theoretical partial cross section to each of all the bound final states. For one-proton knockout from ^{17}N, with a ΔS value of 8.04 MeV, the R_s of 0.56(6) is found to be consistent with the established systematics, as shown in Fig. 5. The R_s of ^{16}C and ^{18}O are also added in the figure. It can be seen that the ^{18}O data point slightly deviates downward from the band of half-width 0.1 (shaded region). It can be seen from Fig. 5 that, there are many cases being outside of the shaded region. Many reasons may lead to this kind of result, such as the uncertainties in the effective interactions used for the calculation of spectroscopic factors C^2S, the nucleon density distribution used for the calculation of S matrices, the rms radius of the valence-proton wavefunctions r_{sp}, and the uncertainties of experimental cross section.

The measured and calculated parallel momentum distributions for the ^{16}C residues and the unreacted ^{17}N nuclei are shown in Fig. 6. For ^{16}C, the red dashed, green dash-dot-dotted, blue dotted, and purple dash-dotted lines represent the calculated parallel momentum distributions for the different bound final states (0_1^+, 0_2^+, 2_1^+, and 2_2^+) after knocking out an $l = 1$ proton from ^{17}N projectiles. The black solid line is the summed theoretical inclusive parallel momentum distribution for the bound final states, which is comparable with the experimental data, represented by the blue solid dots. For ^{17}N, the red solid line is the fitted curve for the measured data, shown with red solid triangles.

For the (^{17}N, ^{16}C) reaction, in an extreme single-particle picture, the p shell of the ^{17}N projectile has five protons: one on the $0p_{1/2}$ orbital and four on the $0p_{3/2}$ orbital. Knocking out one proton from the $0p_{1/2}$ orbital is expected to mainly populate the ^{16}C ground state 0_1^+. The spectroscopic factor

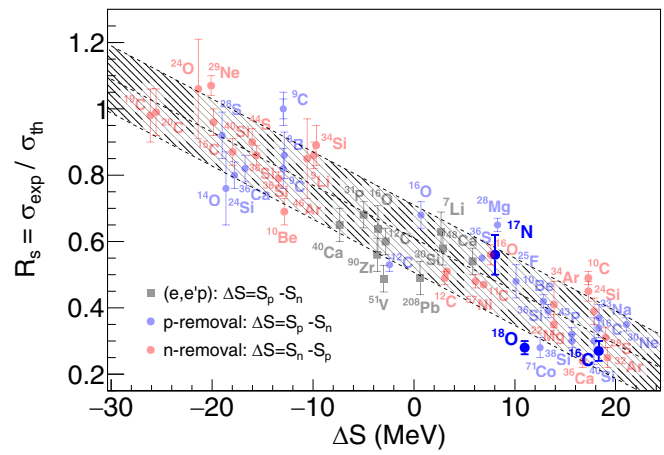

FIG. 5. The R_s value as a function of ΔS. The ^{17}N data are from this work. The experimental one-proton knockout cross sections for ^{16}C and ^{18}O are from Refs. [33] and [34], respectively, and the related theoretical cross sections are from this work. The light-color data points and the R_s-ΔS trend are from Ref. [35].

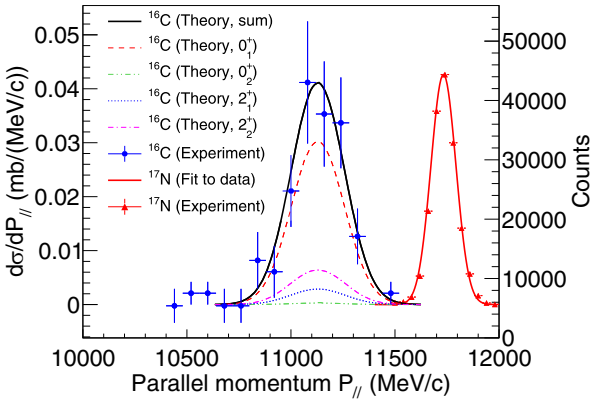

FIG. 6. Measured inclusive parallel momentum distributions for the ^{16}C residues and the unreacted ^{17}N nuclei, represented by the blue solid dots and red solid triangles, respectively. The red solid line is the fitted curve for the measured ^{17}N data, and other curves are different theoretical calculations based on the Glauber model for ^{16}C. See text for further details.

for knocking out one proton from the $0p_{1/2}$ orbital to the ^{16}C ground state is calculated to be 0.76, close to the simple shell model value 1.

By knocking out a proton from the $0p_{3/2}$ orbital of ^{17}N, a series of 2^+ and 1^+ states can be populated. These states are formed by the proton configuration $\pi(0p_{3/2})^3(0p_{1/2})^1$. Among these states, only the first and second 2^+ states are bound. The shell model calculations show that, by knocking out one proton from the $0p_{3/2}$ orbital, the spectroscopic factors to ^{16}C 2^+_1 and 2^+_2 states are 0.08 and 0.18, respectively. As a result, the inclusive spectroscopic factor of knocking out one proton from the $0p_{3/2}$ orbital of ^{17}N to bound states of ^{16}C is 0.26, far less than 4. Much of the spectroscopic strength by knocking out one proton from the $0p_{3/2}$ orbital should feed the unbound states of ^{16}C. Thus, the spectroscopic strength from knocking out a proton from the $0p_{3/2}$ orbital has negligible contribution to the cross section of ^{16}C. When knocking out one proton from the $0p_{3/2}$ or $0p_{1/2}$ orbital, the inclusive spectroscopic factor to bound states of ^{16}C is predicted to be only ≈1, resulting in a small inclusive cross section to bound states of ^{16}C.

For the (^{16}C, ^{15}B) reaction, the projectile ^{16}C has four protons on the $0p_{3/2}$ orbital from a simple shell model picture. The spectroscopic factor for knocking out one proton from the $0p_{3/2}$ orbital to the ^{15}B ground state is predicted to be 2.72, comparable to the simple shell model value 4. For the (^{18}O, ^{17}N) reaction, the projectile ^{18}O has four protons on the $0p_{3/2}$ orbital and two protons on the $0p_{1/2}$ orbital. Knocking out one proton from the $0p_{1/2}$ orbital is predicted to mainly populate the $1/2^-$ ground state of ^{17}N, with a calculated spectroscopic factor of 1.65. By knocking out a proton from the $0p_{3/2}$ orbital, three $3/2^-$ states below neutron separation energy are expected to be populated, with a summed spectroscopic factor of ≈2.9. It can be seen that the inclusive spectroscopic factor for the (^{17}N, ^{16}C) reaction is much smaller than that for the (^{16}C, ^{15}B) and (^{18}O, ^{17}N) reactions, resulting in the smaller inclusive cross section for the (^{17}N, ^{16}C) reaction as compared to the (^{16}C, ^{15}B) and (^{18}O, ^{17}N) reactions.

As the discussion in Refs. [36,37], considering a simple shell model picture, the $1/2^-$ ground state of ^{17}N can be written as

$$|1/2^-;\,^{17}\mathrm{N}\rangle \approx |v(sd)^2; J=0\rangle \otimes |\pi(0p_{3/2})^4(0p_{1/2})^1; J=1/2\rangle\,,$$

with the valence neutrons occupying a quasidegenerate *sd* shell [4]. Additionally, the first excited state 2^+_1 and 0^+_1 ground state of ^{16}C can be expressed by

$$|2^+_1;\,^{16}\mathrm{C}\rangle = \alpha\,|v(sd)^2; J=2\rangle \otimes |\pi(0p_{3/2})^4; J=0\rangle + \beta\,|v(sd)^2; J=0\rangle \otimes |\pi(0p_{3/2})^3(0p_{1/2})^1; J=2\rangle$$

and

$$|0^+_1;\,^{16}\mathrm{C}\rangle = |v(sd)^2; J=0\rangle \otimes |\pi(0p_{3/2})^4; J=0\rangle\,,$$

respectively. Here, α and β respectively are the consituents of pure neutron and pure proton excitations that contribute to the state. Only if one proton is knocked out from the $0p_{1/2}$ orbital of ^{17}N can the 0^+_1 ground state of ^{16}C be populated [14]. As for the knockout of one proton in the $0p_{3/2}$ orbital, the population of 2^+_1 bound state can be fulfilled by the coupling of protons in $0p_{1/2}$ and $0p_{3/2}$ orbitals, with the condition that the proton excitation constituent β is nonzero.

The small spectroscopic factor to the 2^+_1 state indicates that the configuration of the 2^+_1 state has a very small overlap with the proton configuration $\pi(0p_{3/2})^3(0p_{1/2})^1$ and neutron excitation configuration plays a dominant role for the 2^+_1 state.

The presently measured small cross section to ^{16}C combined with theoretical analysis indicates that the majority of ^{16}C residues lie in unbound states after knocking out a proton from the $0p_{3/2}$ orbital of ^{17}N. It suggests that proton excitation in the 2^+_1 state constitutes a small fraction and neutron excitation plays a dominant role, namely, β^2 has a very low numerical value. This is in line with the conclusion in [14]. Following the methodology employed in [14], the values of β^2 are calculated to be 5.0% and 4.3% using the WBP and the YSOX interactions, respectively. The obtained result is related to the calculated spectroscopic factors to the ground and 2^+_1 states of ^{16}C, showing that the result is model dependent.

V. SUMMARY

In summary, the inclusive cross section for one-proton knockout from the neutron-rich nucleus ^{17}N was measured at an energy of 245 MeV/nucleon. The theoretical exclusive cross sections were calculated based on the Glauber reaction model with shell model spectroscopic factors C^2S. It is found that the deduced reduction factor $R_s = \sigma_{\mathrm{exp}}/\sigma_{\mathrm{th}}$ in this work is consistent with the R_s-ΔS systematic established for beam energies mainly at 80–120 MeV/nucleon, implying the robustness of the deduced R_s value to changes in beam energy.

It is found that the experimental one-proton knockout inclusive cross section for ^{17}N is smaller than those for neighboring isotones ^{16}C and ^{18}O. This is because the ^{16}C residue

after knocking out a proton from the $0p_{3/2}$ orbital of ^{17}N is more likely to lie in an unbound state, which is supported by the C^2S results calculated by the shell model. By knocking out a valence proton in the $0p_{3/2}$ orbital of ^{17}N, the summed value of C^2S for related bound states is about 0.26, much smaller than the proton occupation number of 4, indicating that pure proton excitation configuration takes little proportion in the 2_1^+ state of ^{16}C, in agreement with the conclusion of [14].

ACKNOWLEDGMENTS

The authors thank the HIRFL accelerator staff for preparing the primary and secondary beams. This work was supported by the National Natural Science Foundation of China (Grants No. 12305133 and No. 12375186), China Postdoctoral Science Foundation (Grant No. 2023M733575), and the open research project of CAS large research infrastructures.

[1] O. Sorlin and M.-G. Porquet, Prog. Part. Nucl. Phys. **61**, 602 (2008).
[2] T. Otsuka, A. Gade, O. Sorlin, T. Suzuki, and Y. Utsuno, Rev. Mod. Phys. **92**, 015002 (2020).
[3] T. Otsuka, T. Suzuki, M. Honma, Y. Utsuno, N. Tsunoda, K. Tsukiyama, and M. Hjorth-Jensen, Phys. Rev. Lett. **104**, 012501 (2010).
[4] M. Stanoiu *et al.*, Phys. Rev. C **78**, 034315 (2008).
[5] T. Aumann, A. Navin, D. P. Balamuth, D. Bazin, B. Blank, B. A. Brown, J. E. Bush, J. A. Caggiano, B. Davids, T. Glasmacher *et al.*, Phys. Rev. Lett. **84**, 35 (2000).
[6] A. Navin, D. W. Anthony, T. Aumann, T. Baumann, D. Bazin, Y. Blumenfeld, B. A. Brown, T. Glasmacher, P. G. Hansen, R. W. Ibbotson *et al.*, Phys. Rev. Lett. **85**, 266 (2000).
[7] M. G. Mayer, Phys. Rev. **78**, 16 (1950).
[8] D. T. Tran, H. J. Ong, G. Hagen, T. D. Morris, N. Aoi, T. Suzuki, Y. Kanada-En'yo, L. S. Geng, S. Terashima, I. Tanihata *et al.*, Nat. Commun. **9**, 1594 (2018).
[9] J. A. Tostevin and A. Gade, Phys. Rev. C **90**, 057602 (2014).
[10] A. Gade, D. Bazin, B. A. Brown, C. M. Campbell, J. A. Church, D. C. Dinca, J. Enders, T. Glasmacher, P. G. Hansen, Z. Hu *et al.*, Phys. Rev. Lett. **93**, 042501 (2004).
[11] B. A. Brown, P. G. Hansen, B. M. Sherrill, and J. A. Tostevin, Phys. Rev. C **65**, 061601(R) (2002).
[12] D. Bazin, R. J. Charity, R. T. de Souza, M. A. Famiano, A. Gade, V. Henzl, D. Henzlova, S. Hudan, J. Lee, S. Lukyanov *et al.*, Phys. Rev. Lett. **102**, 232501 (2009).
[13] K. Wimmer, D. Bazin, A. Gade, J. A. Tostevin, T. Baugher, Z. Chajecki, D. Coupland, M. A. Famiano, T. K. Ghosh, G. F. Grinyer *et al.*, Phys. Rev. C **90**, 064615 (2014).
[14] M. Petri *et al.*, Phys. Rev. C **86**, 044329 (2012).
[15] P. Hansen and J. Tostevin, Annu. Rev. Nucl. Part. Sci. **53**, 219 (2003).
[16] F. Flavigny, A. Obertelli, A. Bonaccorso, G. F. Grinyer, C. Louchart, L. Nalpas, and A. Signoracci, Phys. Rev. Lett. **108**, 252501 (2012).
[17] Y. Z. Sun, Z. Y. Sun, S. T. Wang, X. H. Zhang, Y. Sun, D. Yan, S. W. Tang, Y. H. Yu, K. Yue, L. M. Duan *et al.*, Nucl. Instrum. Methods Phys. Res., Sect. A **927**, 390 (2019).
[18] J. W. Xia, W. L. Zhan, B. W. Wei, Y. J. Yuan, M. T. Song, W. Z. Zhang, X. D. Yang, P. Yuan, D. Q. Gao, H. W. Zhao *et al.*, Nucl. Instrum. Methods Phys. Res., Sect. A **488**, 11 (2002).
[19] B. H. Sun, J.-W. Zhao, X.-H. Zhang, L.-N. Sheng, Z.-Y. Sun, I. Tanihata, S. Terashima, Y. Zheng, L.-H. Zhu, L.-M. Duan *et al.*, Sci. Bull. **63**, 78 (2018).
[20] W. J. Lin, J.-W. Zhao, B.-H. Sun, L.-C. He, W.-P. Lin, C.-Y. Liu, I. Tanihata, S. Terashima, Y. Tian, F. Wang *et al.*, Chin. Phys. C **41**, 066001 (2017).
[21] X. H. Zhang, S. W. Tang, P. Ma, C. G. Lu, H. R. Yang, S. T. Wang, Y. H. Yu, K. Yue, F. Fang, D. Yan *et al.*, Nucl. Instrum. Methods Phys. Res., Sect. A **795**, 389 (2015).
[22] K. Kimura, T. Izumikawa, R. Koyama, T. Ohnishi, T. Ohtsubo, A. Ozawa, W. Shinozaki, T. Suzuki, M. Takahashi, I. Tanihata *et al.*, Nucl. Instrum. Methods Phys. Res., Sect. A **538**, 608 (2005).
[23] Y. Z. Sun, Z. Y. Sun, S. T. Wang, L. M. Duan, Y. Sun, D. Yan, S. W. Tang, H. R. Yang, C. G. Lu, P. Ma *et al.*, Nucl. Instrum. Methods Phys. Res., Sect. A **894**, 72 (2018).
[24] Y. Sun, Z. Y. Sun, Y. H. Yu, D. Yan, S. W. Tang, Y. Z. Sun, S. T. Wang, X. H. Zhang, K. Yue, F. Fang *et al.*, Nucl. Instrum. Methods Phys. Res., Sect. A **893**, 68 (2018).
[25] C. Wen, Y.-P. Xu, D.-Y. Pang, and Y.-L. Ye, Chin. Phys. C **41**, 054104 (2017).
[26] N. Shimizu, T. Mizusaki, Y. Utsuno, and Y. Tsunoda, Comput. Phys. Commun. **244**, 372 (2019).
[27] E. K. Warburton and B. A. Brown, Phys. Rev. C **46**, 923 (1992).
[28] C. Yuan, T. Suzuki, T. Otsuka, F. Xu, and N. Tsunoda, Phys. Rev. C **85**, 064324 (2012).
[29] Y. Z. Sun and S. T. Wang, Comput. Phys. Commun. **288**, 108726 (2023).
[30] A. Gade, P. Adrich, D. Bazin, M. D. Bowen, B. A. Brown, C. M. Campbell, J. M. Cook, T. Glasmacher, P. G. Hansen, K. Hosier *et al.*, Phys. Rev. C **77**, 044306 (2008).
[31] B. A. Brown, Phys. Rev. C **58**, 220 (1998).
[32] J. S. Al-Khalili, J. A. Tostevin, and I. J. Thompson, Phys. Rev. C **54**, 1843 (1996).
[33] Y. X. Zhao, Y. Z. Sun, S. T. Wang, Z. Y. Sun, X. H. Zhang, D. Yan, D. Y. Pang, P. Ma, Y. H. Yu, K. Yue *et al.*, Phys. Rev. C **100**, 044609 (2019).
[34] X.-D. Xu, Y.-Z. Sun, S.-T. Wang, B. Mei, S.-Y. Jin, X.-H. Zhang, Z.-Y. Sun, Y.-X. Zhao, S.-W. Tang, Y.-H. Yu *et al.*, Chin. Phys. C **46**, 111001 (2022).
[35] J. A. Tostevin and A. Gade, Phys. Rev. C **103**, 054610 (2021).
[36] I. Syndikus, M. Petri, A. O. Macchiavelli, S. Paschalis, C. A. Bertulani, T. Aumann, H. Alvarez-Pol, L. Atar, S. Beceiro-Novo, J. Benlliure *et al.*, Phys. Lett. B **809**, 135748 (2020).
[37] A. O. Macchiavelli, M. Petri, P. Fallon, S. Paschalis, R. M. Clark, M. Cromaz, and I. Y. Lee, Phys. Rev. C **90**, 067305 (2014).